

**Table II. Fractional Atomic Coordinates ( $\times 10^4$ ) and Equivalent Isotropic Temperature Factor Coefficients\* ( $\times 10^3$ ) for [2a][I<sub>5</sub>]**

	x	y	z	U, Å <sup>2</sup>
Re	1974.3 (2)	1604.1 (3)	0.0	30.2 (1)
I(1)	5581.4 (6)	7858.8 (9)	-344.7 (10)	68.2 (4)
I(2)	4063.5 (5)	7149.2 (7)	-626.2 (8)	48.8 (3)
I(3)	2668.6 (7)	6372.9 (9)	-831.0 (10)	64.0 (4)
I(4)	5278.9 (7)	9550.3 (10)	-1942.8 (11)	73.9 (5)
I(5)	4870.9 (7)	10798.9 (9)	-3365.5 (12)	78.1 (5)
P(1)	2737 (2)	200 (3)	156 (4)	57 (1)
P(2)	1254 (2)	2971 (2)	446 (3)	37 (1)
C(1)	2916 (12)	-141 (16)	1377 (19)	90 (10)
C(21)	233 (10)	-907 (12)	-255 (19)	87 (10)
C(3)	3616 (8)	335 (13)	-389 (18)	84 (8)
C(4)	1565 (8)	4125 (8)	31 (14)	53 (5)
C(5)	313 (8)	2916 (12)	130 (15)	66 (6)
C(6)	1239 (9)	3136 (10)	1725 (11)	53 (5)
C(11)	1597 (9)	2085 (10)	-1244 (11)	53 (5)
C(12)	2051 (8)	1313 (11)	-1389 (12)	50 (5)
C(13)	2194 (9)	958 (14)	-2281 (11)	58 (6)
C(14)	1805 (15)	1422 (17)	-2979 (16)	90 (9)
C(15)	1365 (12)	2251 (16)	-2811 (13)	78 (8)
C(16)	1262 (10)	2602 (11)	-1929 (11)	56 (5)
C(17)	2654 (14)	130 (16)	-2586 (16)	94 (8)
C(21)	2826 (6)	2366 (10)	570 (12)	42 (5)
C(22)	3278 (8)	3008 (10)	55 (16)	58 (5)
C(23)	3754 (10)	3562 (12)	594 (16)	70 (7)
C(24)	3828 (11)	3457 (13)	1521 (19)	77 (8)
C(25)	3451 (9)	2797 (13)	2015 (15)	66 (7)
C(26)	2922 (8)	2284 (12)	1560 (14)	59 (6)
C(27)	3215 (12)	3115 (16)	-986 (17)	82 (8)
C(31)	1248 (7)	775 (9)	770 (9)	36 (4)
C(32)	706 (7)	235 (9)	343 (10)	34 (4)
C(33)	237 (7)	-319 (11)	928 (12)	49 (5)
C(34)	359 (10)	-360 (10)	1889 (11)	61 (6)
C(35)	909 (9)	165 (11)	2287 (11)	52 (6)
C(36)	1331 (8)	748 (9)	1722 (10)	44 (4)
C(37)	547 (9)	232 (13)	-710 (12)	60 (6)

\* According to Hamilton (*Acta Crystallogr.* 1959, 12, 609-610).

tracted into hexane (20 cm<sup>3</sup>). Red crystals of **2b** were obtained by concentration and cooling of this solution (0.06 g, 80%).

**X-ray Crystal Structure Determination of [2a][I<sub>5</sub>].** Crystals suitable for X-ray work were grown from dichloromethane/diethyl ether as dark brown needles. The specimen used for the structural work had dimensions 0.22 × 0.30 × 0.70 mm.

Following preliminary photography, the orientation matrix and cell dimensions were obtained by using standard SEARCH and INDEX routines on an Enraf-Nonius CAD4 diffractometer with graphite-monochromated Mo K $\alpha$  radiation ( $\lambda = 0.71069$  Å) and refined by using setting angles for 25 well-spaced reflections with  $9.7 \leq \theta \leq 17.4^\circ$ . The crystal system was found to be orthorhombic, with space group  $Pna2_1$ , and cell dimensions  $a = 18.735$  (2) Å,  $b = 13.954$  (5) Å,  $c = 14.193$  (2) Å,  $V = 3710.6$  Å<sup>3</sup>,  $M_r$  1246.22  $Z = 4$ ,  $D_{\text{calcd}} = 2.23$  g cm<sup>-3</sup>,  $\mu = 73.0$  cm<sup>-1</sup>,  $F(000) = 2284$  at  $T = 291$  K.

Intensity data were recorded by using the  $\omega/2\theta$  scan technique with  $1.5 \leq \theta \leq 25^\circ$ ,  $h = 0 \rightarrow 22$ ,  $k = 0 \rightarrow 16$ ,  $l = 0 \rightarrow 16$ , scan width  $\omega = 0.85 + 0.35 \tan \theta$ , and variable scan speed 1.34 - 6.7 deg min<sup>-1</sup> to achieve  $I \geq 33\sigma(I)$  subject to  $t_{\text{max}} = 60$  s. A total of 3681 data were measured to which 3413 were unique and 2836 observed [ $I > 1.5\sigma(I)$ ]. The data were corrected for absorption empirically; relative maximum and minimum transmission factors were 1.00 and 0.67, respectively. The structure was solved by direct methods (SHELXS 86)<sup>14</sup> and developed and refined by Fourier and full matrix least squares procedures (SHELX 76).<sup>15</sup> All non-hydrogen atoms were refined anisotropically; hydrogens were not included. The final  $R$  and  $R_w$  values were 0.0296 and 0.0417, respectively, for 315 parameters and weights =  $[\sigma^2(F_o) + 0.0002F_o^2]^{-1}$ . The largest  $\Delta/\sigma$  was 0.35 and the minimum/maximum values of  $\Delta\rho$  were  $-0.9/0.7$  e Å<sup>-3</sup>, respectively. The final coordinates are listed in Table II. Refinement of an inverted set of coordinates gave  $R$  and  $R_w$  values of 0.0361 and 0.0452, respectively, confirming the original assignment.

**Acknowledgment.** We thank the SERC for financial support.

**Registry No.** 1, 117407-56-4; **2a**, 117407-50-8; **[2a][PF<sub>6</sub>]**, 117407-53-1; **[2a][BPh<sub>4</sub>]**, 117467-85-3; **[2a][OTf]**, 117467-86-4; **[2a][I<sub>5</sub>]**, 117467-87-5; **2b**, 117407-51-9; **[2b][PF<sub>6</sub>]**, 117407-55-3; **[2b][OTf]**, 117467-88-6; **[2b][Co(CO)<sub>4</sub>]**, 117467-89-7.

**Supplementary Material Available:** Tables of  $U_{ij}$  values and bond lengths and angles (2 pages); a listing of  $F_o/F_c$  values (17 pages). Ordering information is given on any current masthead page.

(14) Sheldrick, G. M. SHELXS 86, Program for crystal structure determination; University of Göttingen: Göttingen, FDR, 1986.

(15) Sheldrick, G. M. SHELX 76, Program for crystal structure calculations; University of Cambridge: Cambridge, England, 1976.

## Deprotonation and Anionic Rearrangement in CpRe(NO)(R)(PPh<sub>3</sub>) (R = CHO, CH<sub>3</sub>)

Maria Clelia Milletti\*<sup>†</sup> and Richard F. Fenske

Department of Chemistry, The University of Wisconsin, Madison, Wisconsin 53703

Received June 6, 1988

The mechanism of migration of the CHO ligand from the metal to the deprotonated cyclopentadienyl ring in  $[(\eta^5\text{-C}_5\text{H}_4\text{Re})(\text{NO})(\text{CHO})(\text{PPh}_3)]^-$  is analyzed from a theoretical point of view. Total energy values for all stable molecules and possible intermediates involved in the reaction are used to determine the lowest energy path. The results are then explained by examining the changes in molecular orbitals occurring during the migration. The fact that alkyl ligands, on the other hand, do not undergo migration to the cyclopentadienyl ligand is also examined.

### Introduction

Gladysz and co-workers have recently observed a series of deprotonation reactions involving rhenium complexes

of the kind CpRe(R)(NO)(PPh<sub>3</sub>), where R = C(O)CH<sub>3</sub>, C(O)C<sub>6</sub>H<sub>5</sub>, C(O)CH<sub>2</sub>C<sub>6</sub>H<sub>5</sub>, C(O)H, H, CH<sub>3</sub>CHCN, (C-H<sub>3</sub>)<sub>2</sub>CH, H<sub>2</sub>CH, H<sub>2</sub>CC<sub>6</sub>H<sub>5</sub>, and H<sub>2</sub>CCH=CH<sub>2</sub>.<sup>1-6</sup> Some

<sup>†</sup> Current address: Department of Chemistry, The University of Michigan, Ann Arbor, MI 48015.

(1) Heah, P. C.; Patton, A. T.; Gladysz, J. A. *J. Am. Chem. Soc.* 1986, 108, 1185.

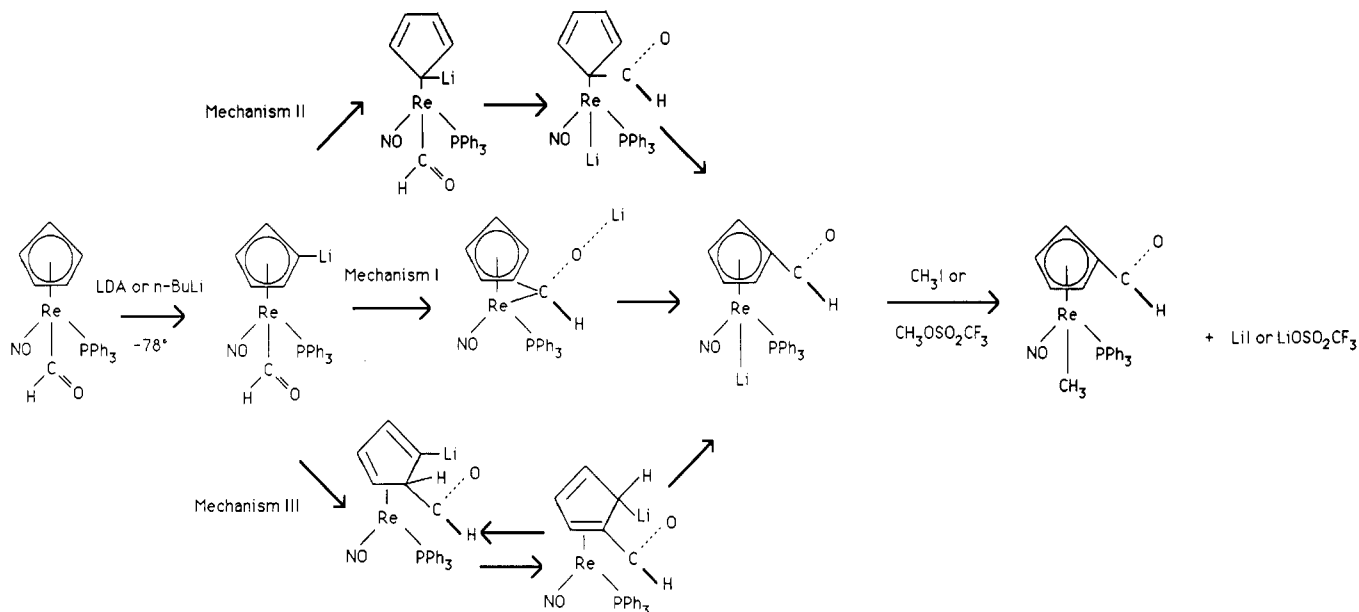


**Figure 1.** Deprotonation reaction and three proposed mechanisms of anionic rearrangement for cyclopentadienylrhenium complexes of the kind CpRe(R)(NO)(PPh<sub>3</sub>) (R = formyl or alkyl).

of such deprotonated cyclopentadienylrhenium compounds subsequently undergo an interesting rearrangement reaction, which involves migration of the R ligand from the metal to the ring (see Figure 1). This migration can be compared and contrasted to similar rearrangements observed in organic systems.<sup>7-10</sup>

Rearrangement reactions of this kind are in fact fairly common in organometallic systems containing a cyclopentadienyl ligand. Several examples of reactions similar to the ones being analyzed in this work can be found in the recent literature. Migration to the cyclopentadienyl ring has been observed for Ge(C<sub>6</sub>H<sub>5</sub>)<sub>3</sub> in CpMo(CO)<sub>3</sub>Ge(C<sub>6</sub>H<sub>5</sub>)<sub>3</sub>,<sup>11</sup> for COCH<sub>3</sub> in CpFe(CO)<sub>2</sub>COCH<sub>3</sub>,<sup>12</sup> and for SiMe<sub>3</sub> in CpFe(CO)<sub>2</sub>SiMe<sub>3</sub>.<sup>13,14</sup> A C-H bond insertion occurs by a similar migration mechanism in CpCr(NO)<sub>2</sub>CH<sub>2</sub>X, when CH<sub>2</sub> inserts in a ring C-H bond.<sup>15</sup>

In the systems that Gladysz and co-workers have investigated, it was observed that migration to the ring will occur only for some of the ligands. For the rearrangements that do occur, three different mechanisms of ligand migration were proposed, but no data are available that would enable one to distinguish between them.<sup>1</sup> The problem at hand is therefore twofold. First, to analyze the three different mechanisms of rearrangement in terms of changes in molecular orbitals and total energy. Once the lowest

energy pathway is identified in such a manner, it can be used to investigate the second part of the problem: why some ligands will undergo the migration and others will not. Or, in other terms, what is the driving force for the intramolecular migration and what factors turn it on and off.

### Computational Procedure

Calculations have been carried out by using the Fenske-Hall nonempirical method<sup>16</sup> on a VAX 8600 computer. The average time required for calculations on each rhenium complex is about 2 min of cpu time. Atomic basis functions were employed; for oxygen, carbon, nitrogen, and phosphorus Clementi's double- $\zeta$  functions were used,<sup>17</sup> except for 1s and 2s functions, which were curve-fit to single- $\zeta$  by using the maximum overlap criterion.<sup>18</sup> The hydrogen exponent was set to 1.16. The rhenium(1+) functions were obtained by performing an atomic X- $\alpha$  calculation on a set of optimized, orthonormal Slater-type orbitals;<sup>19</sup> the 6s and 6p exponents were set to 2.30 to avoid working with metal outer functions that are too diffuse, which often leads to meaningless results.

The total energy of each molecule is calculated by using the Hartree-Fock expression<sup>20,21</sup>

$$E_{\text{HF}} = \sum_{i=1}^{\text{OCC}} \epsilon_i + \sum_{i=1}^{\text{OCC}} \left\langle \Phi_i(1) \left| -\frac{1}{Z} \nabla^2 - \sum_{\alpha} \frac{Z_{\alpha}}{r_{1\alpha}} \right| \Phi_i(1) \right\rangle + \sum_{\alpha} \sum_{\beta} \frac{Z_{\alpha} Z_{\beta} e'^2}{r_{\alpha\beta}} \quad (1)$$

where  $\Phi_i$  is the  $i$ th atomic function. All integrals are calculated within the framework of the same approxima-

(2) Heah, P. C.; Gladysz, J. A. *J. Am. Chem. Soc.* **1984**, *106*, 7636.

(3) Crocco, G. L.; Gladysz, J. A. *J. Chem. Soc., Chem. Commun.* **1985**, 283.

(4) Heah, P. C.; Gladysz, J. A. *J. Mol. Catal.* **1985**, *31*, 207.

(5) Crocco, G. L.; Gladysz, J. A. *J. Am. Chem. Soc.* **1985**, *107*, 4103.

(6) Wong, W.-K.; Tam, W.; Strouse, C. E.; Gladysz, J. A. *J. Chem. Soc., Chem. Commun.* **1979**, 530.

(7) Schollkopf, U. *Angew. Chem., Int. Ed. Engl.* **1970**, *9*, 763.

(8) Pine, S. H. *Org. React. (N.Y.)* **1970**, *18*, 403.

(9) Trost, B. M.; Melvin, L. S., Jr. *Sulfur Ylides*; Academic Press: New York, 1975; Chapter 7, Table A.VII.

(10) Brook, A. G.; Bassindale, A. R. In *Rearrangements in Ground and Excited States*; De Mayo, P., Ed.; Academic Press: New York, 1980; Vol. 2, Essay 9, Table 2.

(11) Dean, W. K.; Graham, W. A. G. *Inorg. Chem.* **1977**, *16*, 1061.

(12) Liebeskind, L. S.; Welker, M. E. *Organometallics* **1983**, *2*, 194.

(13) Berryhill, S. R.; Sharenow, B. *J. Organomet. Chem.* **1981**, *221*, 143.

(14) Berryhill, S. R.; Clevenger, G. L.; Burdurlu, F. Y. *Organometallics* **1985**, *4*, 1509.

(15) Hubbard, J. L.; McVicar, W. K. *J. Am. Chem. Soc.* **1986**, *108*, 6422.

(16) Hall, M. B.; Fenske, R. F. *Inorg. Chem.* **1972**, *11*, 768.

(17) Clementi, E. *J. Chem. Phys.* **1964**, *40*, 1944.

(18) Radtke, D. D. Ph.D. Thesis, University of Wisconsin, Madison, WI, 1966.

(19) Herman, S.; Skillman, S. *Atomic Structure Calculations*; Prentice Hall: Englewood Cliffs, NJ, 1963.

(20) Levine, I. N. *Quantum Chemistry*; Allyn and Bacon, Inc.: Boston, 1983; p 375.

(21) The computer code for subroutine ETOTAL in the Fenske-Hall program MEDIEVAL that is used to calculate total energy values has been developed through a joint effort of Prof. Richard Fenske's and Prof. Bruce Bursten's groups. Details on the total energy modification of the Fenske-Hall method will be disclosed in a future publication.

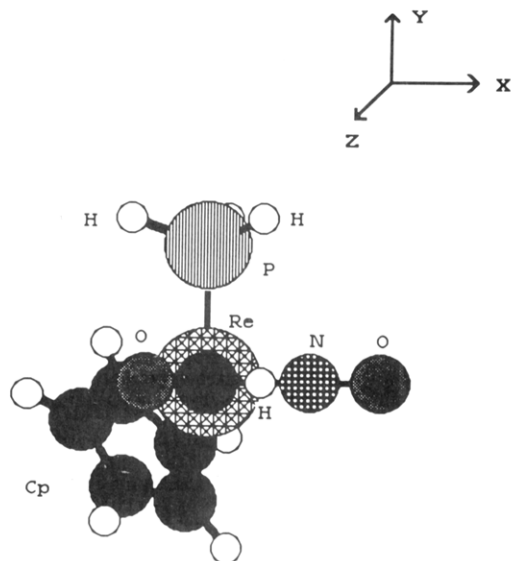


**Figure 2.** Geometry for  $\text{CpRe}(\text{NO})(\text{CHO})(\text{PPh}_3)$  and coordinate system.<sup>24</sup>

tions used in the Fenske–Hall method.<sup>16</sup> Preliminary calculations have been performed to test the validity of the total energy results both by the authors and by Bursten and co-workers.<sup>22</sup> Although the values obtained for the total energies are very large and the energy differences between reactants and products are also too large to be realistic, the trends in the values confirm and follow experimental results. Therefore, the total energy values for the molecules being analyzed should not be taken literally but used for comparison with other complexes in the reaction.

The geometry used for  $\text{CpRe}(\text{NO})(\text{CHO})(\text{PPh}_3)$  is taken from the actual X-ray structure determined by Gladysz et al.<sup>23</sup> and idealized to pseudo- $C_{3v}$  symmetry (see Figure 2). Bond lengths and angles for the other cyclopentadienyl rhenium complexes are extrapolated from the ones in  $\text{CpRe}(\text{NO})(\text{CHO})(\text{PPh}_3)$ . In  $[(\eta^5\text{-C}_5\text{H}_4)\text{Re}(\text{NO})(\text{CHO})(\text{PPh}_3)]^-$  the lithium atom is bonded to the deprotonated carbon of the ring, since this is the site where most of the negative charge is localized. For  $[(\eta^5\text{-CHOC}_5\text{H}_4)\text{Re}(\text{NO})(\text{PPh}_3)]^-$  Gladysz suggests three possible locations of the  $\text{Li}^+$  ion:<sup>1</sup> on the metal, on the formyl oxygen,<sup>25</sup> and on the carbonyl oxygen. In addition, he has found experimental evidence to support the first two possibilities.<sup>26</sup> Calculations were performed on all three configurations. For the intermediate of mechanism I, the lithium atom is bonded to the formyl oxygen and kept in the plane of the formyl ligand, which is roughly parallel to that of the cyclopentadienyl ring. For both intermediates in mechanism III and the first intermediate in mechanism II, the cation

is positioned on the cyclopentadienyl ring; while in the second intermediate of mechanism II the lithium ion is bonded to the metal, in keeping with the results for  $\text{Li}[(\eta^5\text{-CHOC}_5\text{H}_4)\text{Re}(\text{NO})(\text{PPh}_3)]$ . In intermediate 3 of mechanism II (see below), the lithium ion is positioned next to the oxygen of the formyl ligand for  $\text{R} = \text{CHO}$ , in an analogous fashion to what is done for the intermediate of mechanism I. For the methyl compound,  $\text{Li}^+$  is bonded to the oxygen of the nitrosyl group, since this is the atom with the largest negative charge in the anionic complex.

O–Li and C–Li bond lengths have been taken to be 1.59 and 2.01 Å, respectively.<sup>27</sup> The Re–Li bond distance has been optimized and found to be 2.45 Å. For simplicity of interpretation and a greater ease in the calculations, the triphenylphosphine group present in each of the compounds has been substituted with a phosphine group.

## Results and Discussion

**Mechanism of Migration.** For the  $\text{CpRe}(\text{NO})(\text{R})(\text{PPh}_3)$  system, Gladysz has proposed three possible mechanisms of migration,<sup>1</sup> as shown in Figure 1. Currently, though, there is no experimental data available that can differentiate between them. The aim of this first part of the paper, then, is to analyze the intermediates of all three mechanisms by the Fenske–Hall method and, through the results of this analysis, propose which path is the lowest energy one. For the purpose of this work, R will be taken to be CHO.

**Preliminary Considerations.** Before proceeding to the analysis of the actual intermediates in the three different migration pathways, it would be interesting to briefly consider why the initial deprotonation occurs at the cyclopentadienyl ring and not at the CHO ligand. Gladysz has established that the cyclopentadienyl protons are kinetically the most acidic in the related complex  $[(\eta^5\text{-C}_5\text{H}_5)\text{Re}(\text{NO})(\text{H})(\text{PPh}_3)]$ .<sup>26</sup> Furthermore, according to the same author,<sup>1</sup> deprotonation at the ring leads to a more localized carbanion, while deprotonation at the formyl ligand involves rehybridization and charge delocalization. This would imply that the lower energy barrier is the one to the ring carbanion. To test this prediction, calculations were done on both  $[(\eta^5\text{-C}_5\text{H}_4)\text{Re}(\text{NO})(\text{CHO})(\text{PPh}_3)]^-$  and  $[(\eta^5\text{-C}_5\text{H}_5)\text{Re}(\text{NO})(\text{CO})(\text{PPh}_3)]^-$ , where in the second anion CO is kept in the bent conformation. Comparison between these two molecules, therefore, will show the difference between the two types of deprotonation, but without taking into account the need of rehybridization at the formyl ligand.

The results of the calculations show that both anions have similar molecular orbital diagrams. There are, however, a few exceptions. In the case of proton removal from the formyl ligand, the SHOMO (second highest occupied molecular orbital) of the neutral system gets pushed up in energy. This orbital is a metal–formyl bonding orbital, mostly localized on the oxygen of the ligand. In the bent-carbonyl anion it becomes formyl–nitrosyl antibonding and rises in energy to a virtual orbital. On the other hand, the orbital that changes on deprotonation of the ring is a low-energy C–H  $\sigma^b$  orbital on the ring. It is changed to a nonbonding lone-pair orbital on the carbon being deprotonated and rises in energy so that it becomes the HOMO of the anionic system.

(22) Milletti, M. C., Ph.D. Thesis, University of Wisconsin, Madison, WI, 1987, pp 27–31.

(23) Wong, W.-K.; Tam, W.; Gladysz, J. A. *J. Am. Chem. Soc.* **1979**, *101*, 1589.

(24) These diagrams were generated with the help of the program MOLECULAR EDITOR for the Apple Macintosh system, developed by Allan L. Smith, Drexel University.

(25) For the case where the  $\text{Li}^+$  ion is bonded to the oxygen atom of the formyl group, two resonance structures have been taken into account. In the first one, the geometry of the anion remains intact and the cation is positioned 1.59 Å away from the oxygen atom. In the second resonance structure, the  $\pi$ -electron density on the ring is localized on two bonds and the formyl carbon is double bonded to the ring carbon, so that the Li center forms a single bond to the oxygen atom and the metal is coordinated to only four of the ring carbons. For both of these resonance structures it was found that the total energy is higher than for the case of the  $\text{Li}^+$  cation bonded to the metal.

(26) Crocco, G. L.; Gladysz, J. A. *J. Am. Chem. Soc.*, in press.

(27) Casey, C. P., private communication.

(28) At times line connecting sets of two molecular orbitals begin and end between the levels in each set. This is to signify the similar nature of the two orbitals in the set and the fact that often a lot of mixing occurs between them. A consequence of the latter is that there is no one-to-one relationship between orbitals in the beginning and ending sets.

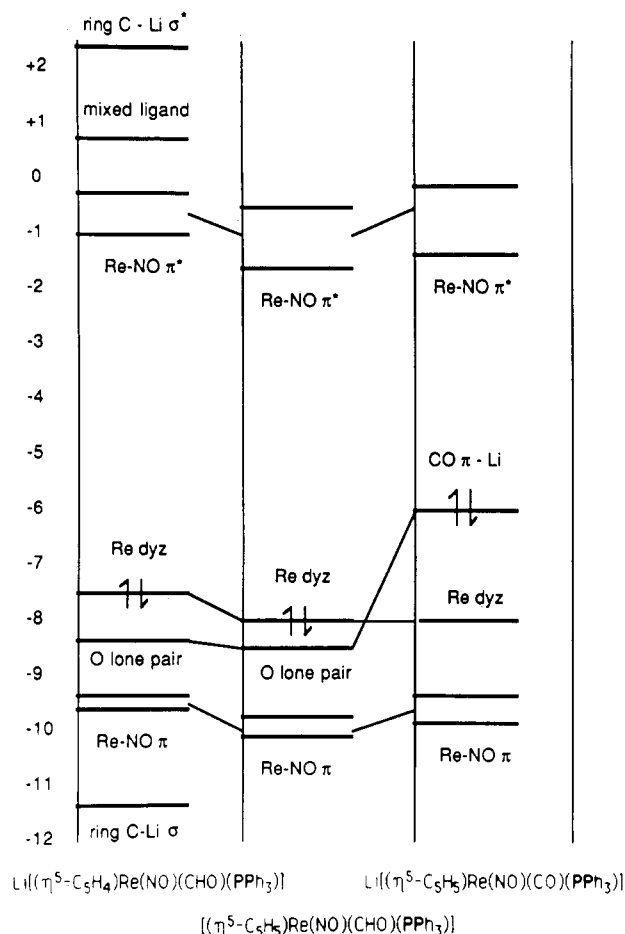


**Figure 3.** Comparison of molecular orbital diagrams for the formyl complex  $CpRe(CHO)(NO)(PPh_3)$  with the two deprotonated salts  $(\eta^5-C_5H_4)Re(CHO)(NO)(PPh_3)$  and  $CpRe(CO)(NO)(PPh_3)$ . Deprotonation at the ring has the net effect to lower one occupied orbital. Therefore it is energetically more favorable than formyl deprotonation, in which the HOMO/LUMO gap is shortened by raising one of the occupied orbitals above the HOMO.<sup>28</sup>

Figure 3 shows what happens to these valence orbitals on formation of the lithium salts. Since all three molecules being analyzed are now neutral, the molecular orbital diagram of the rhenium formyl complex can be included and a direct comparison made. The valence MOs of the neutral formyl complex consist of two  $Re-NO \pi^b$  orbitals, an orbital mostly localized on the oxygen lone pair of the formyl ligand, and a primarily metal d orbital, which is the HOMO of the system. The virtual orbitals of lowest energy are  $Re-NO \pi^*$  in character.

If deprotonation occurs at the Cp ligand, the MO diagram for the lithium salt of the deprotonated molecule shows the formation of a new pair of orbitals: one bonding and one antibonding combination of ring-carbon plus lithium  $\sigma$  orbitals. This pair of orbitals results from the in-phase and out-of-phase combinations of the ring-carbon nonbonding orbital, the HOMO in the anionic species, and the Li 2s. Since the in-phase combination is below the metal-nitrosyl  $\pi^b$  orbital and the out-of-phase combination appears well above the LUMO, the HOMO/LUMO gap of the system is basically left intact from the formyl case.

If deprotonation occurs at the formyl ligand, the MO diagram of the resulting lithium salt again shows only one difference from that of the rhenium formyl: the orbital that was mostly localized on the formyl oxygen lone pair now interacts in a slightly antibonding fashion with the lithium 2s orbital and is therefore raised in energy, be-

coming the HOMO of the system. This is analogous to the energy raising of the oxygen-localized orbital in the anionic system, the major difference being that the nitrosyl participation is now substituted by Li 2s character. The increase in energy of this formyl-localized orbital, which remains occupied, clearly destabilizes the system.

It is clear from Figure 3, then, that the electronic reason why deprotonation at the ring is energetically more favorable is that its net effect is to lower one of the occupied orbitals. This also leaves the HOMO/LUMO gap unchanged,<sup>29</sup> since the new C-Li bond that substitutes the C-H one is sufficiently strong to push the  $\sigma^*$  and  $\sigma^b$  orbitals above and below, respectively, the foremost valence levels. On the other hand, the net effect of formyl deprotonation is out-of-phase mixing of the Li 2s orbital with the formyl C-O  $\pi^b$  orbital, which results in pushing said orbital higher than the HOMO of the neutral rhenium formyl. Therefore, the formyl-deprotonated system is less stable than the ring-deprotonated one.<sup>29</sup>

Total energy calculations on the deprotonated anions also show that the intermediate deprotonated at the ring is more stable than the one deprotonated at the formyl ligand. Both anions are, of course, higher in energy than the neutral formyl complex, but no meaningful comparison can be made between a neutral and an anionic system: the latter will be higher in energy just by virtue of its negative charge. If the neutral complex is compared with the lithium salts of the two anions, it is found that the salts are both lower in energy than the formyl system. Furthermore, the formyl-deprotonated salt is still slightly higher in energy than the cyclopentadienyl-deprotonated salt. Total energy arguments then confirm the conclusions that were previously reached by analysis of valence molecular orbitals.

**$[(\eta^5-C_5H_4)Re(NO)(CHO)(PPh_3)]^-$  and  $[(\eta^5-CHOC_5H_4)Re(NO)(PPh_3)]^-$  and Their  $Li^+$  Salts.** The one feature that the three possible mechanisms of rearrangement have in common is the beginning and end anions involved in the formyl migration: the one with the formyl group still bonded to the metal and the one with the formyl group attached to the ring. It is therefore useful to analyze these two systems first, before comparing the intermediates of the three mechanisms. Figures 4 and 5 show the molecular orbital diagrams for  $[(\eta^5-C_5H_4)Re(NO)(CHO)(PPh_3)]^-$  and  $[(\eta^5-CHOC_5H_4)Re(NO)(PPh_3)]^-$ , respectively.

As previously discussed, the MO diagram of  $[(\eta^5-C_5H_4)Re(NO)(CHO)(PPh_3)]^-$  differs from that of the neutral formyl molecule only in the position of a ring-carbon  $\sigma$  lone-pair orbital, which goes from forming a C-H  $\sigma$  bond to the nonbonding HOMO of the anion upon removal of the proton. The orbitals of interest in Figure 4 are then, starting from the low-energy end, a pair of  $Re-Cp \pi$ -bonding orbitals, a pair of  $Re-NO \pi$ -bonding orbitals, a nonbonding lone-pair orbital of the formyl oxygen, a nonbonding  $Re d_{yz}$  occupied orbital, the ring-carbon lone pair (HOMO), and a pair of  $Re-NO \pi^*$  virtual orbitals.

When the MO diagram for  $[(\eta^5-C_5H_4)Re(NO)(CHO)(PPh_3)]^-$  is compared to the valence molecular orbitals in  $[(\eta^5-CHOC_5H_4)Re(NO)(PPh_3)]^-$  (Figure 5), the first noticeable difference is that the formyl oxygen lone-pair orbital and the  $Re-NO \pi^b$  levels interchange their order. More importantly, the  $Re d-p$  hybrid orbital that used to form a  $\sigma$  bond with the formyl group is left nonbonding after migration of this group to the ring. This rhenium nonbonding orbital now rises in energy and mixes in with

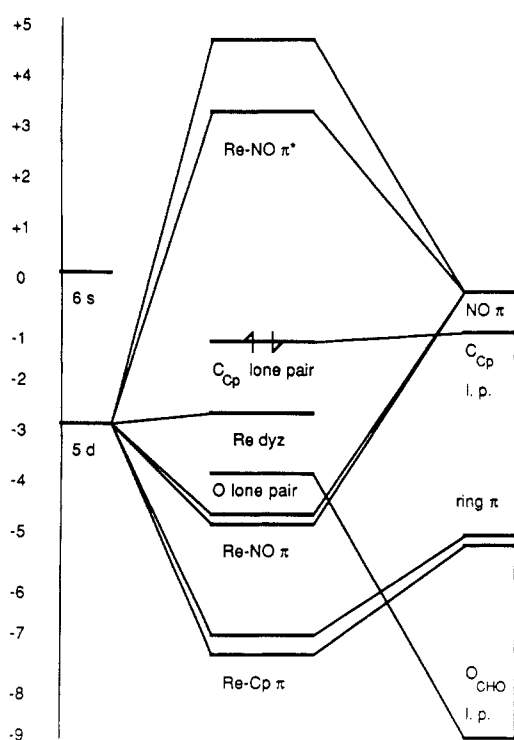


Figure 4. Molecular orbital diagram for  $[(\eta^5\text{-C}_5\text{H}_4)\text{Re}(\text{NO})\text{-(CHO)}(\text{PPh}_3)]^-$ .

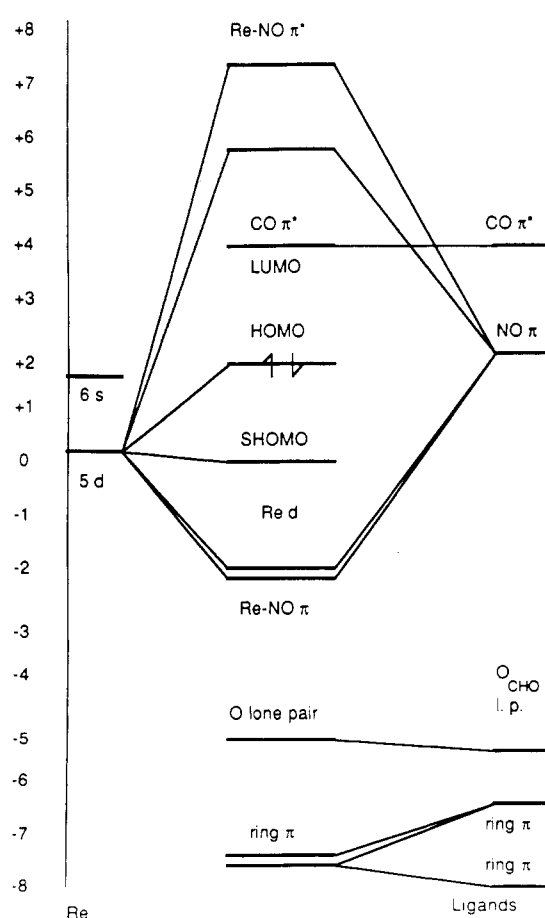


Figure 5. Molecular orbital diagram for  $[(\eta^5\text{-CHOC}_5\text{H}_4)\text{Re}(\text{NO})(\text{PPh}_3)]^-$ .

the Re  $d_{yz}$  orbital to form two metal-based,  $d_{yz}\text{-}d_{z^2}$  orbitals that are the HOMO and the SHOMO of the system. The other main difference with the  $[(\eta^5\text{-C}_5\text{H}_4)\text{Re}(\text{NO})\text{-(CHO)}(\text{PPh}_3)]^-$  MO diagram is the energy lowering of the

Table I. Total Energies for Possible Bonding Sites of  $\text{Li}^+$  on  $[(\eta^5\text{-CHOC}_5\text{H}_4)\text{Re}(\text{NO})(\text{PPh}_3)]^-$

	total energy, eV
Li on Re	-450 535.575
Li on formyl O	-450 395.202
Li on nitrosyl O	-450 404.360

formyl C-O  $\pi^*$  orbital, which becomes the LUMO of the ring-formylated molecule. This is due to the fact that the antibonding  $\pi$  interactions with Re d orbitals that used to push the C-O  $\pi^*$  orbital to higher energy disappear when the formyl group is on the ring.

In  $[(\eta^5\text{-CHOC}_5\text{H}_4)\text{Re}(\text{NO})(\text{PPh}_3)]^-$ , the formyl group has been positioned parallel to the plane of the ring because this leads to the most stable configuration. In the molecular orbital sequence for the  $(\text{CHOC}_5\text{H}_4)^{3-}$  ligand the HOMO is a  $\pi^*$  orbital on C-O, while the LUMO is an antibonding combination of ring carbons  $p_x$ 's and  $p_y$ 's. If the formyl group is flipped so that it is perpendicular to the ring, the HOMO and the LUMO of the system become almost degenerate; due to this almost negligible HOMO/LUMO gap, the perpendicular configuration is very unstable.<sup>28</sup> The increase in energy of the C-O  $\pi^*$  orbital is the result of loss of  $\pi$  delocalization with the ring that occurs when the formyl  $\pi$  system becomes perpendicular to that of the ring.

The effect of adding a  $\text{Li}^+$  ion to both of the anions being analyzed is an overall lowering of all the valence molecular orbitals. In addition, the lithium cation actually bonds to the ring carbon in  $\text{Li}[(\eta^5\text{-C}_5\text{H}_4)\text{Re}(\text{NO})(\text{CHO})(\text{PPh}_3)]$ , and this causes the HOMO of the anion to split into a bonding, low-energy C-Li orbital and an antibonding, virtual C-Li orbital. In  $\text{Li}[(\eta^5\text{-CHOC}_5\text{H}_4)\text{Re}(\text{NO})(\text{PPh}_3)]$ , three different bonding sites for the cation have been considered. Following Gladysz's suggestions,<sup>1</sup> calculations have been carried out for the cases where  $\text{Li}^+$  is bonded to the nitrosyl oxygen, to the formyl oxygen,<sup>24</sup> and to the rhenium center. This last configuration was found to be by far the most energetically stable one, while the first two possibilities had similar, but higher, total energy values (see Table I).

**Mechanism I.** Mechanism I involves a smooth migration of the formyl group from the metal to the cyclopentadienyl ring. Only one intermediate is present, where the formyl group is halfway between the metal and the ring and the H-C=O plane is roughly parallel to that of the ring. Unfortunately, in the molecular orbital diagram for the intermediate a lot of mixing occurs and there is no clear-cut character to the orbitals. Addition of  $\text{Li}^+$  does very little to change the sequence of molecular orbitals; the Li 2s orbital remains basically nonbonding as a high-lying virtual orbital.

Because of the high degree of mixing present in the system, it is very difficult to follow the reaction through changes in the molecular orbitals; an alternative way of viewing mechanism I is to look at overlap populations. Overlap populations are calculated according to eq 2,<sup>30</sup>

$$P(k,l) = \sum_i^{\text{OCC}} \sum_r \sum_s 2N(i)C_{rk}C_{sl}S(r_k,s_l) \quad (2)$$

where  $N(i)$  is the occupation of the  $i$ th molecular orbital,  $r$  is an atomic orbital on center  $k$ , and  $s$  is an atomic orbital on center  $l$ ,  $C$ 's are eigenvectors, and  $S$  is an overlap integral. Since eq 2 sums over all interactions between two centers in the occupied orbitals, it recovers the total bonding and antibonding interaction between the two

(30) De Kock, R. L. Ph.D. Thesis, University of Wisconsin, Madison, WI, 1970.

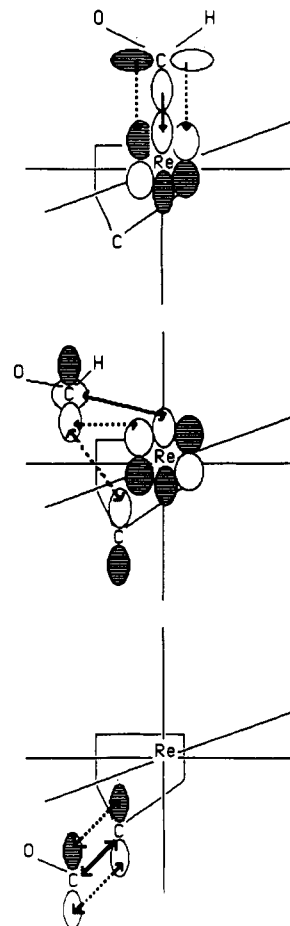
**Table II. Overlap Populations of Formyl Carbon with Other Centers in Mechanism I<sup>a</sup>**

Reactant					
	Re 5d <sub>z<sup>2</sup></sub>	Re 5d <sub>yz</sub>	Re 6s	Re 6p <sub>z</sub>	H 1s
C 2s	<i>0.09928</i>	0.00000	0.02735	0.01256	<i>0.31586</i>
C 2p <sub>x</sub>	0.00000	0.00000	-0.02813	0.00000	<i>0.42352</i>
C 2p <sub>y</sub>	0.00000	<i>0.11747</i>	0.00000	0.00000	0.00000
C 2p <sub>z</sub>	<i>0.15468</i>	0.00000	<i>0.11352</i>	<i>0.15384</i>	<i>0.11435</i>
Intermediate					
	Re 5d <sub>z<sup>2</sup></sub>	Re 5d <sub>yz</sub>	Re 6s	Re 6p <sub>z</sub>	H 1s
C 2s	0.00027	<i>0.09115</i>	-0.04919	-0.05259	<i>0.25816</i>
C 2p <sub>x</sub>	0.00000	0.00123	0.00475	0.00000	<i>0.27555</i>
C 2p <sub>y</sub>	<i>0.11203</i>	-0.01692	0.00000	-0.01217	<i>0.23740</i>
C 2p <sub>z</sub>	0.00221	0.04213	0.03654	0.01155	-0.00932
Product					
	Re 5d <sub>z<sup>2</sup></sub>	Re 5d <sub>yz</sub>	Re 6s	Re 6p <sub>z</sub>	H 1s
C 2s	0.00992	0.00000	0.02735	0.01256	<i>0.27771</i>
C 2p <sub>x</sub>	0.00000	0.00000	-0.02813	0.00000	<i>0.38024</i>
C 2p <sub>y</sub>	0.00000	0.01174	0.00000	0.00000	0.00000
C 2p <sub>z</sub>	<i>0.01546</i>	0.00000	0.01135	0.01538	<i>0.14350</i>

<sup>a</sup>Numbers showing significant overlap have been emphasized (italicized) for clarity.

centers that has been dispersed by the mixing due to a lowering of symmetry.

On the formyl group, the orbitals to be followed throughout the reaction are C 2p<sub>z</sub>, which can form  $\sigma$  bonds, and C 2p<sub>y</sub>, which will form  $\pi$  bonds. Table II shows the carbon atomic orbitals overlap populations with the other centers in the molecule. The table clearly shows that, besides overlap with the formyl hydrogen and oxygen atomic orbitals, the carbon center overlaps with rhenium only in the reactant, with rhenium and the ring in the intermediate, and with the ring only in the product. This broadly agrees with the movement of the formyl group throughout the reaction. More specifically, in the reactant C 2s and 2p<sub>z</sub>  $\sigma$  bond with the rhenium d<sub>z<sup>2</sup></sub>, 6s, and 6p<sub>z</sub> orbitals and C 2p<sub>y</sub>  $\pi$  bonds with the rhenium d<sub>yz</sub> orbital.

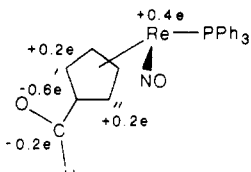


**Figure 6.** Overlap changes throughout mechanism I. Solid arrows indicate p<sub>z</sub> or s overlaps, and dotted arrows indicate p<sub>y</sub> overlaps. The formyl group initially interacts with the metal center only, in both a  $\pi$  and  $\sigma$  fashion. It then moves to a bridging position, where it uses its p<sub>y</sub> orbital to bond with both the metal and the ring carbon. In the product, the formyl group is bonded only to the ring carbon.

In the intermediate, C 2s  $\sigma$  bonds with the rhenium d<sub>yz</sub> orbital, while C 2p<sub>y</sub> bonds with both Re d<sub>z<sup>2</sup></sub> and ring C 2s and 2p<sub>y</sub>, thus forming a "bridge" between the two centers. In the product, formyl C 2s and 2p<sub>z</sub>  $\sigma$  bond to ring C 2s and 2p<sub>z</sub>, while p<sub>y</sub> orbitals on both centers form the  $\pi$  bond.

Figure 6 illustrates pictorially the results obtained from the overlap populations; the formyl group starts out by interacting with the metal, in both a  $\pi$  and  $\sigma$  fashion, with its filled p<sub>z</sub> and empty p<sub>y</sub> atomic orbitals. It then moves on to an intermediate position, in which it can be considered a bridging group, where it uses its p<sub>y</sub> orbital to interact both with the metal and the ring carbon. In the product, the formyl carbon bonds, again in both a  $\sigma$  and  $\pi$  fashion, to the ring carbon. Unlike the Re d orbital, though, the ring C 2p<sub>z</sub> orbital already has a pair of electrons, and the formyl C 2p<sub>z</sub> orbital must therefore be empty. The two electrons that it originally contained have been left, in part, on the metal, in what now are the HOMO and the SHOMO of the molecule. A look at Mulliken atomic charges confirms this analysis. As can be seen from Table III, the rhenium center gains 0.4 electron, which comes in equal parts from the formyl and ring carbons (-0.2 electron each). Furthermore, 0.4 additional electron is lost by the ring carbon to the two carbons adjacent to it.

**Mechanism II.** The distinctive feature of mechanism II is that it involves intermediates where the ring is bound to the metal in an  $\eta^1$  fashion. The key to understanding molecular orbital changes in this mechanism, therefore, is to analyze the changes involved in going from an  $\eta^5$  to

**Table III. Comparison of Mulliken Atomic Charges for Mechanism I**


	reactant	intermediate	product
Re	0.166	0.422	-0.233
C <sub>CHO</sub>	0.050	0.092	0.288
C <sub>Cp</sub>	-0.687	-0.370	-0.076
C <sub>Cp'</sub>	0.143	0.115	-0.074
C <sub>Cp''</sub>	0.198	0.202	-0.013

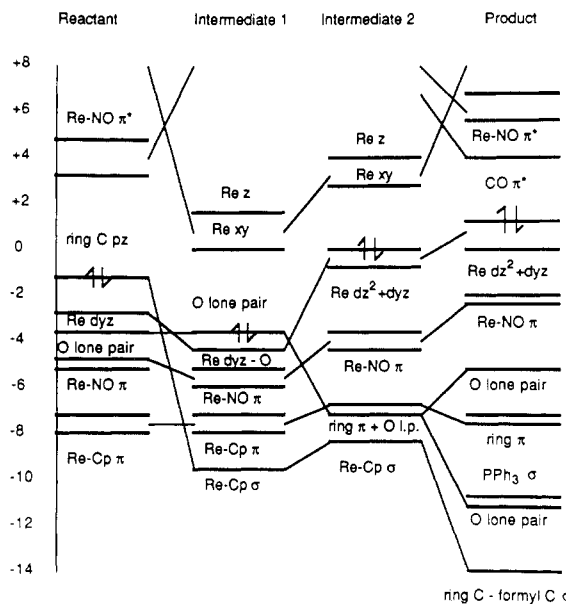
an  $\eta^1$  ring and back. The formyl migration occurs while the ring is in an  $\eta^1$  position. When analyzing changes in molecular orbitals, it is best to look at the anions first, since the added influence of a  $\text{Li}^+$  ion that continuously changes position can be confusing. Later, when the basic mechanism is understood, the counterion can be added on in order to obtain a more complete picture.

Figure 7 follows the changes in the molecular orbitals of the anions for mechanism II. Going from the reactant to the first intermediate, the Cp ring slips to an  $\eta^1$  position. This causes the lone pair on the ring carbon (HOMO in the reactant) to drop in energy because of  $\sigma$  bonding with Re d orbitals. Furthermore, loss of metal-ring  $\pi$  interaction causes Re s and p orbitals, which used to be pushed up by  $\pi$  antibonding interactions, to drop down in energy and mix with Re empty d levels. Consequently, the LUMO is now an empty metal orbital in the  $x$ - $y$  plane. The Re  $d_{yz}$  and O lone-pair levels, which are close in energy in the reactant, change order in the first intermediate because of some mixing between them, so that the O lone pair is left as the HOMO.

The changes occurring between intermediates 1 and 2 are due to the formyl group migrating to the ring. The two  $\pi$  ring levels mix with the formyl oxygen lone pair to form two new levels that are still primarily ring  $\pi$  in character, but with some O lone-pair contribution. The Re  $d_{yz}$  orbital is no longer stabilized by the formyl oxygen, and the  $d_{z^2}$  orbital is no longer  $\sigma$  bonded to the formyl carbon. These two levels are raised in energy and mix together to form the SHOMO and HOMO of the second intermediate. The LUMO is still the empty Re orbital.

When the formylated ring goes back to the  $\eta^5$  position, ring C  $\sigma$  bonding to the metal becomes mostly a ring-formyl  $\sigma$  bond, which lowers the orbital considerably.  $\pi$  interaction with the ring ligand is restored, and the Re-NO  $\pi^*$  orbitals are now lower than the Re p orbitals, but the formyl C-O  $\pi^*$  orbital is also lowered and becomes the LUMO of the system. The two ring  $\pi$  orbitals that had some O lone-pair contribution are again stabilized by interaction with the metal, while the O lone-pair character splits out into two distinct orbitals.

Last, let us consider the effect of adding a  $\text{Li}^+$  ion on the four molecules involved in mechanism II. As previously discussed, in the reactant the lithium ion forms a very strong  $\sigma$  bond with the ring-deprotonated carbon, giving rise to a very low-energy  $\sigma^b$  and a very high-energy  $\sigma^*$  orbital. In the first intermediate, on the other hand, the Li 2s orbital remains nonbonding and virtual; the rest of the molecular orbitals remains intact but are all lowered in energy. In intermediate 2, the ion bonds to the metal, causing the HOMO/SHOMO pair to split into two bonding and two antibonding orbitals. The higher energy one of the bonding pair is mostly localized on the metal and



**Figure 7.** Comparison of the molecular orbitals of anions in mechanism II. In the reactant the lowest unoccupied orbitals are Re-NO  $\pi^*$ . But in the two intermediates a pair of nonbonding metal-based orbitals drop in energy because of the loss of  $\pi$  interaction with the ring and become the lowest unoccupied orbitals. The HOMO of the reactant is the  $p_z$  lone pair on the deprotonated ring carbon. This orbital bonds with the metal center in the intermediates and drops in energy, leaving oxygen and Re lone pairs as the HOMO. In the product, the formylated ring goes back to an  $\eta^5$  position and the formyl C-O  $\pi^*$  orbital becomes the LUMO.<sup>28</sup>

remains the HOMO of the molecule. In the product, again the Li 2s orbital remains mostly nonbonding and there is just a general lowering of all the valence orbitals.

**Mechanism III.** In the third mechanism, the formyl group migrates to the ring in the first intermediate, but to a position adjacent to the carbon that has been deprotonated. In the second intermediate, the formyl group moves to its final position by "trading places" with the  $\text{Li}^+$  ion, and finally the lithium ion migrates to the metal in the last step.

Again, the mechanism will first be followed through the anionic complexes. Figure 8 shows how the comparison diagram for mechanism III is overall simpler than that for mechanism II. As a first approximation, the Re-NO  $\pi^b$  and  $\pi^*$  levels are more or less constant in energy throughout the reaction. The orbital that is the lone pair on the ring deprotonated carbon remains high in energy for the first half of the reaction, when the formyl group is still bonded to the metal. In the reactant it is the HOMO and in the first intermediate the SHOMO of the system. Subsequently, this level drops drastically in energy because of  $\sigma$  bonding to the formyl group. In the second intermediate there is no clear level that is ring-formyl bonding; the overlap populations, though, show a total of 0.849 23 for  $2s$ ,  $2p_x$ - $2s$ ,  $2p_z$  overlap and 0.105 88 for  $2p_y$ - $2p_y$  overlap between the ring and the formyl carbons. In the product, a single bonding orbital appears again at low energy.

Another orbital that stays fairly constant throughout the reaction is the nonbonding C-O  $\pi^*$  level. One noticeable fact, which is also apparent in mechanism II, is the drop in energy of this orbital whenever the formyl moves from the metal to the ring. This is due to antibonding interactions between the C-O  $\pi^*$  level and the metal. C-O  $\pi^*$  therefore makes up the LUMO of all molecules in this mechanism, except for the reactant, in which it is split into two high-lying Re-CO antibonding levels. The metal

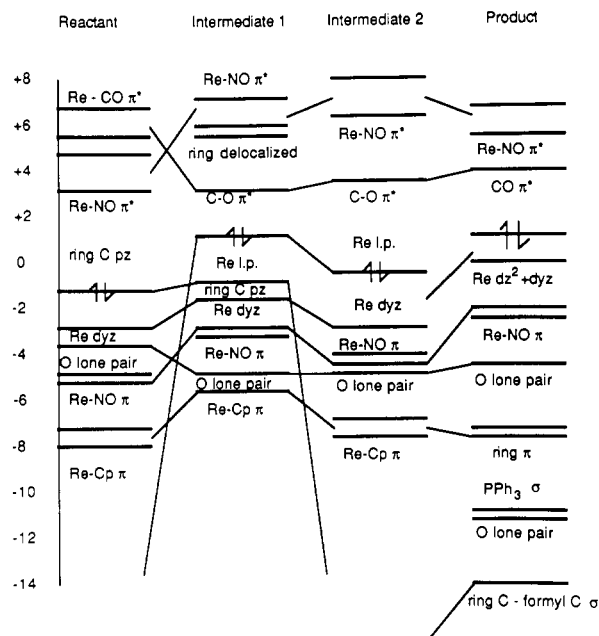


**Figure 8.** Comparison of molecular orbitals of anions for mechanism III. In the reactant the LUMO is again  $Re-NO \pi^*$ . Once the ring is formylated, in the first intermediate, the formyl  $C-O \pi^*$  orbital is lowered in energy and becomes the LUMO. The HOMO of the reactant is still the lone pair on the ring carbon. Once the formyl group moves to the ring, the metal lone-pair orbital that is left behind shoots up in energy and becomes the HOMO of the system.<sup>28</sup>

center shows a  $d_{yz}$  orbital that remains mostly nonbonding, except for some mixing with another metal lone pair in the second half of the reaction. This other lone pair is a  $d-p$  hybrid oriented in the positive  $z$  direction that is involved in  $\sigma$  bonding with the formyl group in the reactant and subsequently remains nonbonding. The reactant shows no single orbital that is  $Re-C_{CHO} \sigma$  bonding, but overlap populations show a total of 0.521 32 between  $Re d_{z^2}$ ,  $s$ ,  $p_z$  and  $C_{CHO} s$ ,  $p_z$ .

As far as the influence of the lithium ions on the anions just analyzed is concerned, the patterns for the reactant and product are, of course, the same as in mechanism II and they have already been discussed. Both intermediates show that the lithium ion is either nonbonding or in very high- or low-energy orbitals and the effects seen are, for the most part, a general lowering of the already existing orbitals. In intermediate 1 there is a mixing of the three highest occupied molecular orbitals, which are all metal-based. The mixing occurs because the  $C_{Cp}$  character that was present in two of them disappears when the  $Li^+$  ion bonds to that carbon. The  $C_{Cp}-Li \sigma^b$  and  $\sigma^*$  orbitals are too low and high in energy, respectively, to be among the valence orbitals. In the second intermediate, there is some mixing of the  $C-O \pi^*$  and  $Li 2s$  levels, which leads to a raising of the former and a lowering of the latter.

**Preferred Mechanism.** Now that the three mechanisms have been analyzed from a molecular orbital point of view, it is time to decide which one is energetically more favored. To do this, total energy arguments will be used followed by another look at the MO diagrams to decide what makes one mechanism favored over the others.

Figure 9 shows an overall view of the total energies of the neutral salts involved in the reaction. Anions are not shown because of the difficulty in comparing complexes with different overall charges. The initial deprotonation is a downhill step, as the neutral formyl complex is at higher energy than the corresponding lithium salt. Of the three possible mechanisms that follow, the second one

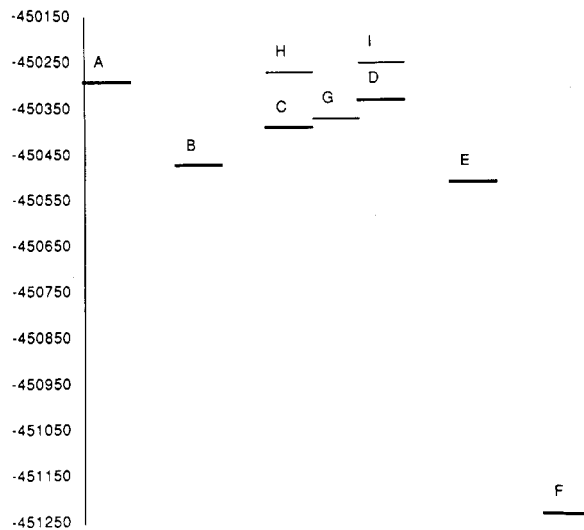


**Figure 9.** Overall energy comparison: A,  $[(\eta^5-C_5H_5)Re(NO)(CHO)(PPh_3)]$ ; B,  $Li[(\eta^5-C_5H_4)Re(NO)(CHO)(PPh_3)]$ ; C, lithium salt of intermediate 1, mechanism II; D, lithium salt of intermediate 2, mechanism II; E,  $Li[(\eta^5-CHOC_5H_4)Re(NO)(PPh_3)]$ ; F,  $[(\eta^5-CHOC_5H_4)Re(NO)(CH_3)(PPh_3)]$ ; G, lithium salt of intermediate of mechanism I; H, lithium salt of intermediate 1, mechanism III; I, lithium salt of intermediate 2, mechanism III. The reaction follows the energies in bold.

seems to be energetically favored, since its first intermediate is lower in energy than the first intermediate of the other two mechanisms. It should be noted, though, that while the intermediates for mechanism III are at much higher energy than those of mechanism II, mechanism I goes through an intermediate which is energetically between those of mechanism II. Therefore, mechanism I still remains a possibility that cannot be totally ruled out. For the hydride complex  $[(\eta^5-C_5H_5)Re(NO)(H)(PPh_3)]$ , Gladysz has found both thermodynamic and kinetic data to be consistent with mechanism I. Although mechanisms II and III could not be rigorously excluded, the latter is considered the least likely possibility.<sup>26</sup>

After proceeding through the two intermediates of mechanism II (the first at a lower energy than the second), the reaction comes back down for the lithium salt with the formylated ring. This complex is at a lower energy than the corresponding one with the lithiated ring. The methyl compound, which is the thermodynamic product of the reaction, is at a much lower energy than any of the previously discussed molecules.

Further insight into the problem can be obtained by analyzing the various contributions to the total energy of the intermediates for all three mechanisms. Clearly, both the sum of orbital energies and nuclear-nuclear repulsion terms contribute to making mechanism II the lowest energy path, while the  $KE + NA$  ( $KE =$  kinetic energy;  $NA =$  nuclear attraction) term puts it at the highest energy of all three mechanisms. The trends for nuclear-nuclear repulsion are easily rationalized: mechanism I has the only intermediate with a high positive value for this term because of the in-between position of the formyl group. On the other hand, mechanism II has lower values than mechanism III because the  $\eta^1$  slip in mechanism II takes the ring "out of the way" of the rest of the molecule.

As far as the sum of orbital energies contribution is concerned, analysis of valence MOs in each complex leads to the explanation for lower energy for mechanism II (refer to Figures 7 and 8). In this mechanism, the high-lying lone pair on the ring carbon is greatly stabilized by bonding with the metal center, while in mechanism III it remains nonbonding (the formyl initially migrates to the adjacent



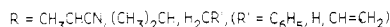
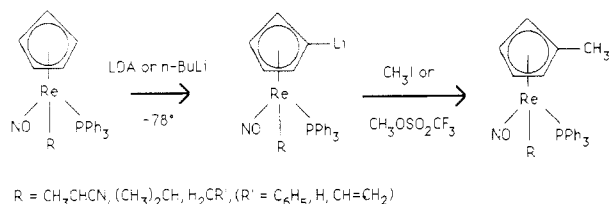


**Figure 10.** Deprotonation and subsequent methylation reaction for  $\text{CpRe}(\text{NO})(\text{R})(\text{PPh}_3)$ , ( $\text{R} = \text{alkyl or aryl}$ ).

position on the ring). In mechanism I it is slightly destabilized by an antibonding interaction with the oxygen of the formyl group. On the other hand, the Re orbital that bonds with the formyl group in  $\text{Li}[(\eta^5\text{-C}_5\text{H}_4)\text{Re}(\text{NO})(\text{CHO})(\text{PPh}_3)]$  is greatly destabilized in the first intermediate of mechanism III because of the migration of the formyl group itself, which does not occur in mechanism II until the second intermediate.

The answer to the question of why the methyl compound is so much more stable than any of the other complexes is that the large increase in electron-electron repulsion due to substitution of a  $\text{Li}^+$  cation with a methyl cation is counteracted by a large stabilization of the  $\text{KE} + \text{NA}$  term. Contributions to the net total stabilization, then, come almost in equal proportions from the  $\text{KE} + \text{NA}$  and sum of orbital energies terms. In particular, the HOMO of  $\text{Li}[(\eta^5\text{-CHOC}_5\text{H}_4)\text{Re}(\text{NO})(\text{PPh}_3)]$  is substantially stabilized by replacement of the  $\text{Li}^+$  ion with the  $\text{CH}_3^+$  moiety. Substituting a methyl group for  $\text{Li}^+$  has the primary effect of taking the HOMO ( $\text{Re } d_{z^2} + d_{yz}$ ) and stabilizing it through bonding with the empty carbon orbital on  $\text{CH}_3^+$ . The  $\text{Re } d_{yz}$  orbital is therefore left as the HOMO, while the LUMO is still  $\text{C-O } \pi^*$  in character, causing an increase in the HOMO/LUMO gap.

Such stabilization does not occur when the metal is bonded to  $\text{Li}^+$  for two reasons. There is slightly better overlap between the rhenium lone pair and the methyl empty p-type orbital (0.95) than between the rhenium lone pair and the  $\text{Li } 2s$  orbital (0.93), but, more importantly, the energy match between  $\text{Re } d$  and methyl  $p$  ( $\Delta E = 1.43$  eV) is better than the match between  $\text{Re } d$  and  $\text{Li } 2s$  ( $\Delta E = 3.97$  eV). Another consequence of the fact that the  $\text{Re-CH}_3$  bond is more covalent than the  $\text{Re-Li}$  bond used to be is that some of the charge on the metal in the lithium salt is transferred to the methyl carbon in the methyl rhenium complex ( $\text{Re}$ , from  $-0.635$  to  $-0.031$ ;  $\text{Li}$ , 0.230;  $\text{C}_{\text{CH}_3}$ ,  $-0.271$ ).

In summary, then, mechanism II has been found to be the lowest energy path. The features that favor this mechanism are the  $\eta^5$  to  $\eta^1$  slip of the cyclopentadienyl ring which minimizes nuclear-nuclear repulsions and the fact that the formyl migration does not occur until the second intermediate, thus allowing the  $\text{Re } d_{z^2}$  level to remain low in energy during the initial step.

**Ligands That Do Not Migrate.** Now that the mechanism of migration of the R group in  $\text{CpRe}(\text{NO})(\text{R})(\text{PPh}_3)$  is understood, the next step is to consider the types of R groups that do not undergo migration. Gladysz has observed that  $\text{CH}_3\text{CHCN}$ ,  $(\text{CH}_3)_2\text{CH}$ , and  $\text{H}_2\text{CR}$  (where  $\text{R} = \text{C}_6\text{H}_5$ ,  $\text{H}$ ,  $\text{CH}=\text{CH}_2$ ) do not migrate to the anionic site on the cyclopentadienyl ligand, so that, in the subsequent reaction with  $\text{CH}_3\text{I}$ , the methyl group attacks the ring rather than the metal center<sup>1</sup> (see Figure 10).

The purpose of this section is to consider orbital and energetic differences between formyl-type and alkyl-type groups; the nature of such differences will then be used to explain why an alkyl group cannot migrate to the cyclopentadienyl ring in the same way as formyl groups do.

For the purpose of this investigation,  $\text{CH}_3$  will be used as the prototype for an alkyl group.

To better understand the effects of changing R from CHO to  $\text{CH}_3$ , the alkyl ligand is first assumed to undergo migration in the same way the formyl ligand does. Fenske-Hall calculations were carried out on all of the complexes in Figure 1 (except for the intermediates of mechanisms I and III) and their corresponding anions, with  $\text{CH}_3$  substituted for CHO. Considering mechanism II only is justified by the results of the preceding section, where the other two mechanisms were ruled out because found to be energetically less favorable.

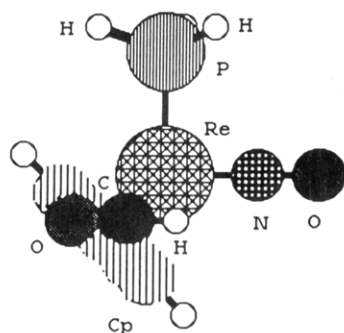
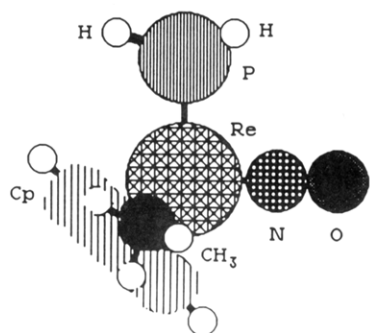
When a plot of the total energies for the molecules involved in the reaction is compared with the analogous plot for  $\text{R} = \text{CHO}$  shown in Figure 9, very little difference between the energetics of the two reactions is found. It is clear, then, that the difficulty alkyl ligands show in migrating to the cyclopentadienyl ring must have its roots in the lack of  $\pi$ -accepting character which is present in the formyl ligand. The formyl group has the advantage of being bonded to an electronegative atom such as oxygen to which it can shift electron density. This movement of electrons away from the carbon atom undergoing the migration helps to stabilize the system while the migrating group is moving to the lone pair on the ring carbon atom and, at the same time, is still partially bonded to the metal center.

To better investigate the role that  $\pi$ -accepting capability plays in the migration process, it is then necessary to take a closer look at the intermediate stage in which the R group is "bridging" between metal and ring. In the course of mechanism II, this point occurs between the two intermediates in a configuration which is not itself a stable intermediate, rather more of an activated complex. For the sake of convenience, though, it will be referred to as intermediate 3. The geometry of this configuration is similar to that of the first intermediate in mechanism II, but the position of the R group is that found in the intermediate of mechanism I (see Figure 11).

Figures 12 and 13 show the molecular orbital diagrams for intermediate 3,  $\text{R} = \text{CHO}$  and  $\text{CH}_3$ , respectively. Overall, both diagrams show a high degree of mixing of the atomic orbitals, which is appropriate for species of such low symmetry and which was also apparent in the MO diagrams of the intermediate of mechanism I. Again, the major difference between the two types of molecules is the lack of oxygen lone-pair and  $\text{C-O } \pi^*$  orbitals in the methyl complex.

The foremost valence orbitals in the  $\text{R} = \text{CH}_3$  case are a metal-ring  $\pi$ -antibonding orbital (SHOMO), an antibonding orbital which has rhenium-mixed-ligand character (HOMO), an orbital which is mostly  $\text{Re } d_{z^2}$  with some ring antibonding interaction (LUMO), and the usual pair of  $\text{Re-NO } \pi^*$  orbitals at much higher energies. The striking feature of Figure 13 is the very small HOMO/LUMO gap, while the HOMO/SHOMO separation and the separation between the LUMO and the next unoccupied orbital are comparatively very large; all this points to the instability of the methyl system.

The formyl complex shows a similar orbital configuration, but the  $\text{Re } d_{z^2}$  orbital, which is the LUMO of the  $\text{R} = \text{CH}_3$  system, is now interacting in a bonding fashion with the  $\text{C-O } \pi^*$  orbital of the formyl group. This causes the molecular orbital to drop down in energy and to become the HOMO of the system; the  $\text{Re}$ -mixed-ligand antibonding orbital is left as the LUMO and the HOMO/LUMO gap is thus increased with respect to the one for the methyl system.

a.  $R = CHO$ b.  $R = CH_3$ 

**Figure 11.** Geometries for intermediate 3 of mechanism II ( $R = CHO$  and  $CH_3$ ).<sup>24</sup>

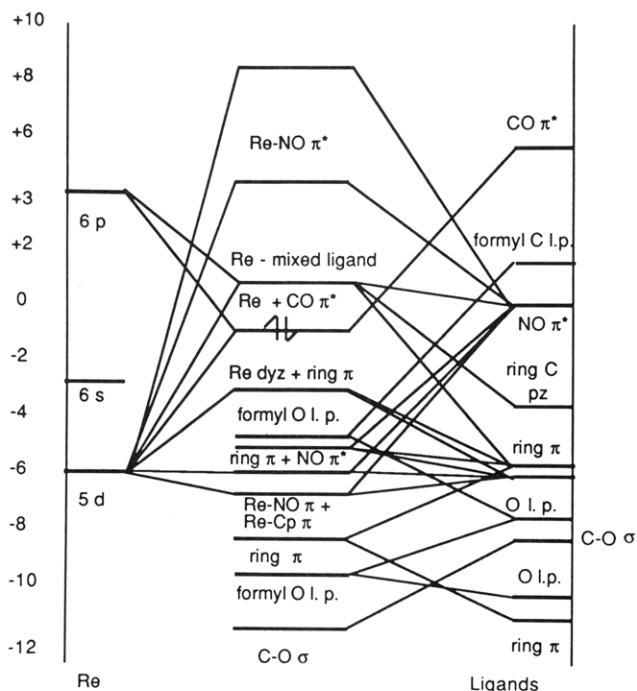


**Figure 12.** Molecular orbital diagram for the anion of intermediate 3 ( $R = CHO$ ).

The molecular orbital diagrams for the corresponding lithium salts are in all similar to the ones for the anions, except for the addition of a mostly nonbonding Li 2s orbital. This lithium empty orbital gets pushed up above the LUMO by electrostatic interaction with the oxygen atom it is closest to and ends up between the  $Re-NO \pi^*$  orbitals for  $R = CHO$  and just below them for  $R = CH_3$ .

In conclusion, then, the prediction made earlier in this section about the reason why the methyl ligand does not

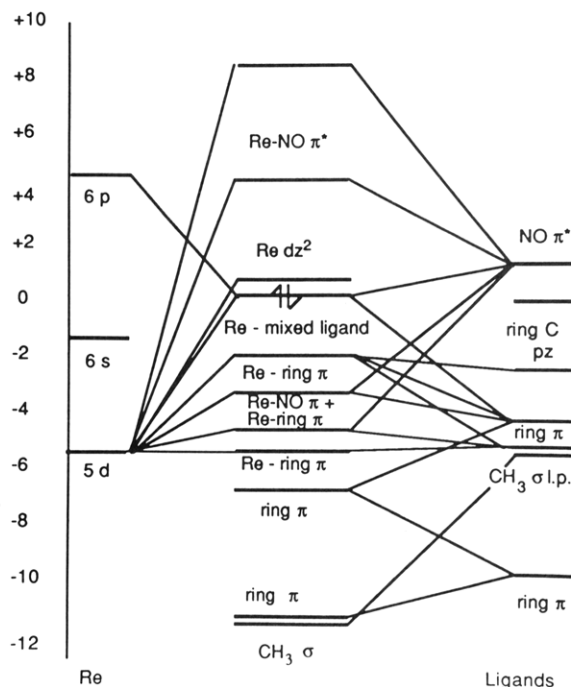


**Figure 13.** Molecular orbital diagram for the anion of intermediate 3 ( $R = CH_3$ ). Notice the very small HOMO/LUMO gap that points to the instability of the system.

migrate has been proven correct by analysis of the molecular orbital diagrams. The presence of a  $C-O \pi^*$  unoccupied orbital at a fairly low energy on the formyl ligand allows for displacement of some charge on the electronegative oxygen atom, which stabilizes the intermediate stages of ligand migration. This shift of charge density is not possible on an alkyl-type ligand, which makes the migration an unfavorable process for  $R = CH_3$ . This conclusion is further supported by a variety of experimental evidence that the best migrating ligands should have low-lying acceptor orbitals.<sup>1,14,31</sup>

### Conclusions

In the introduction of this paper it was stated that the theoretical investigation of the problem would lead to an appreciation of what drives the migration and the factors that turn it on and off. In order to evaluate these points, it is useful to review the results of the foregoing investigation and summarize what has been learned about the intramolecular migration under consideration.

Gladysz suggests that the formylated ring compound is a kinetic product, while the product of the subsequent methyl attack is thermodynamic in kind.<sup>1</sup> Figure 9 shows that this is indeed the case, with  $[(\eta^5-CHOC_5H_4)Re(NO)(CH_3)(PPh_3)]$  at a much lower energy than  $Li[(\eta^5-CHOC_5H_4)Re(NO)(PPh_3)]$ . Formation of the latter molecule can then be considered the driving force for the migration. Analogously, Berryhill et al. have suggested that formation of the coordinatively unsaturated 18-electron anion in the  $CpFe(CO)_2(SiMe_3)$  system may drive the rearrangement.<sup>14</sup>

Furthermore, the factor that seems to be crucial in order for a ligand to be able to migrate is  $\pi$ -accepting ability. The important step in the migration is at the intermediate position of the migrating ligand between the metal and the ring. In this phase the extra charge from the ring carbon has to be shifted away from the migrating carbon; only the presence of an electronegative center on the migrating

ligand can accomplish this. Furthermore, the  $\pi$ -accepting empty orbital offers an ulterior mode of bonding that facilitates bridging between the two centers. All of these factors make the formyl ligand a better migrating group than the alkyl ligand. When R = H, the migration still occurs, but more slowly;<sup>3</sup> even though the hydrogen atom has no electronegative center bonded to it, the spherical

symmetry of its orbital still allows for fair bridging capabilities.

**Acknowledgment.** We thank Prof. Charles P. Casey for many helpful discussions and we are grateful to the National Science Foundation for financial support through Grant No. CHE-8601434.

## A Simple Route to Hexacarbonyldiiron Complexes Containing a Bridging Thiolate and an Organic Bridging Ligand by Means of $[(\mu\text{-RS})(\mu\text{-CO})\text{Fe}_2(\text{CO})_6]^-$ Intermediates

Dietmar Seyferth,\* Gary B. Womack, Colin M. Archer, and John C. Dewan

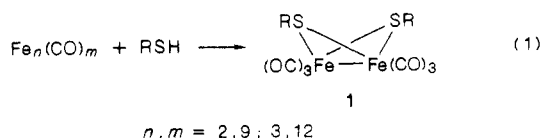
Department of Chemistry, Massachusetts Institute of Technology, Cambridge, Massachusetts 02139

Received June 9, 1988

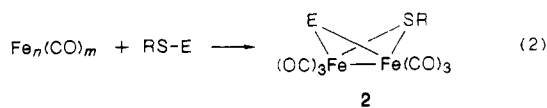
The reaction of thiolate salts,  $\text{M}^+\text{SR}^-$ , with  $\text{Fe}_3(\text{CO})_{12}$  in THF at room temperature gives  $\text{M}[(\mu\text{-CO})(\mu\text{-RS})\text{Fe}_2(\text{CO})_6]$ . These react as nucleophiles at the oxygen of the bridging CO ligand (with  $\text{Et}_3\text{O}^+\text{BF}_4^-$ ) and as nucleophiles at iron (with halides of potentially bridging groups:  $\text{RC}(\text{O})\text{Cl}$ ,  $\text{Me}_2\text{NC}(\text{S})\text{Cl}$ , allyl chloride, propargylic halides) to give products of type  $(\mu\text{-RS})(\mu\text{-organic group})\text{Fe}_2(\text{CO})_6$  in good yield. A less practical route to such products involves the action of 2 molar equiv of  $\text{LiBEt}_3\text{H}$  on  $(\mu\text{-CH}_3\text{CO})(\mu\text{-RS})\text{Fe}_2(\text{CO})_6$ , followed by addition of the halide electrophile. The reaction of the  $[(\mu\text{-CO})(\mu\text{-RS})\text{Fe}_2(\text{CO})_6]^-$  anions with propargylic halides was shown to proceed by way of an  $\text{S}_{\text{N}}2'$  mechanism. The structures of  $[\text{Et}_3\text{NH}](\mu\text{-CO})(\mu\text{-mesitylS})\text{Fe}(\text{CO})_6$ ,  $(\mu\text{-allyl})(\mu\text{-C}_2\text{H}_5\text{S})\text{Fe}_2(\text{CO})_6$ , and  $(\mu\text{-allenyl})(\mu\text{-}(\text{CH}_3)_3\text{CS})\text{Fe}_2(\text{CO})_6$  were determined by X-ray diffraction.

### Introduction

Diiron hexacarbonyl complexes containing two bridging thiolate ligands are readily prepared as shown in eq 1.<sup>1</sup>



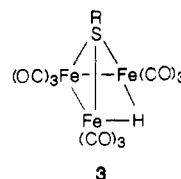
However, dinuclear complexes containing a bridging RS group in conjunction with a different type of bridging ligand are not readily accessible. The reaction shown in eq 2 serves this purpose, and examples are known where



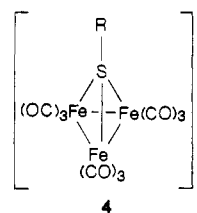
E is  $\text{R}'_2\text{P}$ ,<sup>2</sup>  $\text{CH}_2=\text{CH}$ ,<sup>3</sup>  $\text{R}'\text{SC}(\text{S})$ ,<sup>4</sup>  $\text{R}'\text{OC}(\text{S})$ ,<sup>5</sup>  $\text{R}'\text{C}(\text{NR}'')$ ,<sup>6</sup> and  $\text{R}'\text{C}\equiv\text{C}$ .<sup>7</sup> Such reactions generally give only poor-to-moderate product yields, and, furthermore, the starting RS-E compound is not always easily available. We report here the development of a new method of preparation of

complexes of type 2 which does not require the prior synthesis of an RS-E compound, a reaction which is based instead on the reactivity of an intermediate formed by the action of thiolate anions,  $\text{RS}^-$ , on triiron dodecacarbonyl.

The first report of the reaction between organic thiols and  $\text{Fe}_3(\text{CO})_{12}$ , by Hieber and Spacu in 1937,<sup>8</sup> provided examples of the reaction shown in eq 1. Many complexes of type 1 have been reported since that time.<sup>1</sup> Reactions of secondary and tertiary thiols with  $\text{Fe}_3(\text{CO})_{12}$  also gave trinuclear complexes of type 3.<sup>9</sup> Such complexes could



be deprotonated with a tertiary amine, and the resulting anionic species 4 reacted with a variety of electrophiles,



for instance,  $\text{R}_2\text{PCl}$ ,  $\text{R}_2\text{AsCl}$ ,  $\text{RPCl}_2$ , and  $\text{Cl}_2$ , to give new  $\text{Fe}_3(\text{CO})_9$  cluster complexes.<sup>10</sup> In related work, Takács and

(1) *Gmelin Handbook of Inorganic Chemistry*, 8th ed.; Springer-Verlag: Berlin, 1978; Organoiron Compounds, Part C1, pp 77-93.

(2) (a) Mathey, F.; Comarond, M.-B.; Moran, D. *J. Chem. Soc., Chem. Commun.* 1979, 417. (b) Job, R. E.; McLean, R. A. N.; Thompson, D. T. *J. Chem. Soc., Chem. Commun.* 1966, 1895.

(3) King, R. B.; Treichel, P. M.; Stone, F. G. A. *J. Am. Chem. Soc.* 1961, 83, 3600.

(4) Patin, H.; Mignani, G.; Mahé, C.; LeMarouille, J.-Y.; Southern, T. G.; Benoit, A.; Grandjean, P. *J. Organomet. Chem.* 1980, 197, 315.

(5) Patin, H.; Mignani, G.; Benoit, A.; LaMarouille, J.-Y.; Grandjean, D. *Inorg. Chem.* 1981, 20, 4351.

(6) Seyferth, D.; Hoke, J. B. *Organometallics* 1988, 7, 524.

(7) Seyferth, D.; Hoke, J. B., unpublished work.

(8) Hieber, W.; Spacu, P. Z. *Anorg. Allg. Chem.* 1937, 233, 353.

(9) (a) deBeer, J. A.; Haines, R. J. *J. Chem. Soc., Chem. Commun.* 1970, 288. (b) deBeer, J. A.; Haines, R. J. *J. Organomet. Chem.* 1970, 24, 757.